The Third Family of Compact Objects as a Tool to Constrain the Nuclear Equation of State

L. Tsaloukidis[1], **P.S. Koliogiannis**[2], **A. Kanakis-Pegios**[2], **Ch.C. Moustakidis**[2]

[1]Max Planck Institute for the Physics of Complex Systems (MPI-PKS) and Würzburg-Dresden Cluster of Excellence ct.qmat. 01187 Dresden, Germany

[2]Department of Theoretical Physics, Aristotle University of Thessaloniki, 54124 Thessaloniki, Greece

Abstract. In agreement with the constantly increasing gravitational wave events, new aspects of the internal structure of compact stars can be considered. A scenario in which a first order transition takes place inside these stars is of particular interest as it can lead, under conditions, to a third gravitationally stable branch (besides white dwarfs and neutron stars), the twin stars. In the present work, we focus on hybrid stars undergone a hadron to quark phase transition near their core and how this new stable configuration arises. Emphasis is to be given on the aspects of the phase transition and its parametrization in two different ways, namely with Maxwell and Gibbs construction. We systematically study the gravitational mass, the radius, and the tidal deformability, and we compare them with the predictions of the recent observation by LIGO/Virgo collaboration, the GW170817 event, along with the mass and radius limits, suggesting possible robust constraints. Finally, we discuss the constraints on the radius and mass of the recently observed compact object within the supernova remnant HESS J1731-347. The estimations imply that this object is either the lightest neutron star known, or a star with a more exotic equation of state.

1 Introduction

Compact stars yield the most prominent natural laboratories for the study of exotic forms of matter [1–4]. Recently discovered pulsars alongside with gravitational waves detection, such as GW170817, have revealed new aspects of the internal structure of these stars, mainly in terms of their composition [5–7]. Whilst the equation of state (EoS) of nuclear matter is well established up to nuclear saturation density, one encounters the challenge of describing matter in fairly higher densities realized in the interior of these stars. At these densities the type of matter is yet to be determined and in turn, the construction of stellar models to agree with the aforementioned observations is still an open issue. Possible candidates are pure neutron stars composed by hadrons, strange quark stars composed of deconfined quarks, and hybrid stars composed by hadronic outer shells and cores of deconfined quarks. Stars of this branch are expected to

have masses in the same range as normal neutron stars, yet fairly smaller radii. The existence of such stars is a strong indication that a hadron-quark phase transition (HQPT) is a physical reality, a result of utmost importance, especially in the study of dense matter physics [8–10].

The idea of a third family of compact stars and in particular, the connection with the possibility to be a signature of a strong phase transition in the interior of the star, was firstly introduced by Gerlach [11]. Later on, Kämpfer worked also on this issue [12, 13]. Glendenning and Kettner introduced the term "twins" in their paper [14], while at the same time Schertler *et al.* [15] worked out that idea in detail. However, in all the previous studies, the maximum mass was approximately at the canonical binary pulsar mass $1.4\ M_\odot$. The revival of the idea of the twin stars started a few years later by Blaschke *et al.* [16,17]. Specifically, in the mentioned papers is suggested that high-mass twin stars, once detected by simultaneous mass and radius measurements, could provide the evidence for a strong first-order phase transition in cold matter, which then would imply the existence of at least one critical endpoint in the quantum chromodynamics phase diagram. The previous idea was elaborated by Benic *et al.* [18] (see also Ref. [19]). A systematic Bayesian analysis of the new twin star EoS with observational constraints was presented in Ref. [20].

One of the motivations of the present work is to examine in a more systematic way the applications of the two main formulation of the phase transition, that is the Maxwell (MC) and Gibbs (GC) constructions. These formulations are quite different, as the former imposes an energy jump between the two phases while the latter implements a smooth transition between the phases. Finally, we employ the constraints on mass and radius of the recently observed compact object within the supernova remnant HESS J1731-347 [21]. The corresponding estimations are $M = 0.77^{+0.20}_{-0.17}\ M_\odot$ and $R = 10.4^{+0.86}_{-0.78}$ km, respectively. According to the authors' guess, the above estimates imply that this object is either the lightest neutron star known, or a star with a more exotic equation of state. In any case, it is worth considering to what extent this compact object is compatible with the hybrid model and thus with the twin stars theory.

The paper is organized as follows. In Section 2 we present the basic formalism of the hadron to quark phase transition. In Section 3 we provide the tidal deformability while the Section 4 is dedicated to the presentation and discussion of the results of the present study.

2 Hadronic to Quark Matter Phase Transition

2.1 Maxwell construction

The first case is the well-known MC case, which exhibits a sharp transition according to the following ansatz [8–10]

$$\mathcal{E}(P) = \begin{cases} \mathcal{E}_{\mathrm{HADRON}}(P), & P \le P_{\mathrm{tr}} \\ \mathcal{E}(P_{\mathrm{tr}}) + \Delta\mathcal{E} + c_s^{-2}(P - P_{\mathrm{tr}}), & P \ge P_{\mathrm{tr}}. \end{cases} \tag{1}$$

47

In the above formula $\mathcal{E}(P)$ denotes the energy density, P the pressure, $c_s = \sqrt{\partial P / \partial \mathcal{E}}$ the speed of sound in units of speed of light, and $\Delta\mathcal{E}$ the magnitude of the energy density jump at the transition point. During the quark phase the numerical value we assign for c_s is equal to $c_s = 1$, the maximum allowed value that is consistent with causality. That way we also ensure the stiffest EoS case and the greatest possible range of M-R relations. Moreover, P_{tr} expresses the pressure that corresponds to the baryon density at phase transition point, n_{tr}.

2.2 Gibbs construction

The Gibbs phase transition rule regarding the equality of the pressure of the two components (Hadron - Intermediate, Intermediate - Quark) is established here. Contrary to the MC case, where the pressure remains constant in the transition interval, in the GC case, the pressure increases with increasing baryon density, while also no discontinuities in the energy density appear, giving rise to the profile [10]

$$\mathcal{E}(P) = \begin{cases} \mathcal{E}_{\mathrm{HADRON}}(P), & P \leq P_{\mathrm{tr}}, \\ A_{\mathrm{m}} \left(P/K_{\mathrm{m}} \right)^{1/\Gamma_{\mathrm{m}}} + \gamma_{\mathrm{m}} P, & P_{\mathrm{tr}} \leq P \leq P_{\mathrm{CSS}}, \\ \mathcal{E}(P_{\mathrm{CSS}}) + c_s^{-2}(P - P_{\mathrm{CSS}}), & P \geq P_{\mathrm{CSS}}, \end{cases} \tag{2}$$

where $A_{\mathrm{m}} = 1 + \alpha_{\mathrm{m}}$, $\gamma_{\mathrm{m}} = (\Gamma_{\mathrm{m}} - 1)^{-1}$, and $c_{\mathrm{s}} = 1$ (maximally stiff EoS). The energy density is denoted by $\mathcal{E}(P)$, the pressure by P, the speed of sound by c_{s}, while a_m, K_m and the polytropic index Γ_m are constants, with the former two evaluated, by requiring continuity of P and $\mathcal{E}$ at the transition points.

2.3 Seidov criterion

The phase transition from the hadronic matter to the quark matter described in the previous section is set to produce an instability in the star when a certain criterion is met. This critical value, was derived by Seidov [22] and reads as

$$\Delta\mathcal{E}_{\mathrm{cr}} = \frac{1}{2}\mathcal{E}_{\mathrm{tr}} + \frac{3}{2}P_{\mathrm{tr}}. \tag{3}$$

In order to have a third family of compact objects appear in the M-R diagram, the aforementioned instability has to be satisfied. In order to be able to compare the GC with the MC, where an energy jump appears in the form of $\Delta\mathcal{E}_{\mathrm{cr}}$, we define the corresponding energy increase in the GC as the quantity

$$\Delta\mathcal{E}_{\mathrm{G}} = \frac{3}{2}\left(\frac{1}{2}\mathcal{E}_{\mathrm{HADRON}}(P_{\mathrm{tr}}) + \frac{3}{2}P_{\mathrm{tr}}\right), \tag{4}$$

with $\mathcal{E}_{\mathrm{HADRON}}(P_{\mathrm{tr}})$ and P_{tr} representing the respective values at the transition from the hadron phase to the mixed phase.

3 Tidal Deformability

A very important source for the gravitational wave detectors are the gravitational waves from the late phase of the inspiral of a binary neutron star system, before the merger [23–25]. This kind of source leads to the measurement of various properties of neutron stars. In the inspiral phase the tidal effects can be detected [24].

The k_2 parameter, also known as tidal Love numbeer, depends on the equation of state and describes the response of a neutron star to the tidal field E_{ij} [24]. The exact relation is given below

$$Q_{ij} = -\frac{2}{3}k_2\frac{R^5}{G}E_{ij} \equiv -\lambda E_{ij}, \tag{5}$$

where R is the neutron star radius and $\lambda = 2R^5 k_2/3G$ is the tidal deformability. The tidal Love number k_2 is given by [24, 25]

$$
\begin{aligned}
k_2 \;=\; & \frac{8\beta^5}{5}\left(1-2\beta\right)^2\left[2-y_R+(y_R-1)2\beta\right] \\
\times\; & \Big[\,2\beta\left(6-3y_R+3\beta(5y_R-8)\right) \\
+\; & 4\beta^3\left(13-11y_R+\beta(3y_R-2)+2\beta^2(1+y_R)\right) \\
+\; & 3\left(1-2\beta\right)^2\left[2-y_R+2\beta(y_R-1)\right]\ln\left(1-2\beta\right)\Big]^{-1},
\end{aligned}
\tag{6}
$$

where $\beta = GM/Rc^2$ is the compactness of a neutron star. The paramter y_R is determined by solving numerically the following differential equation

$$r\frac{dy(r)}{dr} + y^2(r) + y(r)F(r) + r^2Q(r) = 0, \tag{7}$$

with the initial condition $y(0) = 2$ [26]. $F(r)$ and $Q(r)$ are functionals of the energy density $\mathcal{E}(r)$, pressure $P(r)$, and mass $M(r)$. Eq. (7) must be solved numerically and self consistently with the Tolman - Oppenheimer - Volkoff (TOV) equations under the following boundary conditions: $y(0) = 2$, $P(0) = P_c$ (P_c denotes the central pressure), and $M(0) = 0$ [23, 25]. From the numerical solution of TOV equations, the mass M and radius R of the neutron star can be computed, while the corresponding solution of the differential Eq. (7) provides the value of $y_R = y(R)$. The last parameter along with the quantity β are the basic ingredients of the tidal Love number k_2.

The chirp mass $\mathcal{M}_c$ of a binary neutron stars system is a well measured quantity by the gravitational wave detectors [7]. Its relation is given below

$$\mathcal{M}_c = \frac{(m_1 m_2)^{3/5}}{(m_1 + m_2)^{1/5}} = m_1\frac{q^{3/5}}{(1+q)^{1/5}}, \tag{8}$$

where m_1 is the mass of the heavier component star and m_2 is the lighter's one. Hence, the binary mass ratio $q = m_2/m_1$ lies within the range $0 < q \le 1$.

Additionally, another quantity that is well measured is the effective tidal deformability $\tilde{\Lambda}$ which is given by [7]

$$\tilde{\Lambda} = \frac{16}{13} \frac{(12q+1)\Lambda_1 + (12+q)q^4\Lambda_2}{(1+q)^5}, \tag{9}$$

where Λ_i is the dimensionless tidal deformability [7]

$$\Lambda_i = \frac{2}{3}k_2 \left(\frac{R_i c^2}{M_i G}\right)^5 \equiv \frac{2}{3}k_2\beta_i^{-5}, \quad i = 1, 2. \tag{10}$$

The effective tidal deformability $\tilde{\Lambda}$ is one of the main quantities that can be well measured by the detection of the corresponding gravitation waves.

4 Results and Discussion

In our study, as we have already mentioned, we used two constructions, a) the MC, and b) the GC, and two different EoSs, a) the MDI+APR1 EoS [27], and b) the GRDF-DD2 EoS [28]. Also, we focused on the following values of $n_{tr} = [0.20, 0.25, 0.30, 0.32, 0.35, 0.38, 0.43, 0.50]$ fm^{-3}. In particular, Figures 1 and 2 indicate the MDI+APR1 EoS with the MC and GC, respectively, while similar figures are taken for the GRDF-DD2 EoS with the MC and GC,
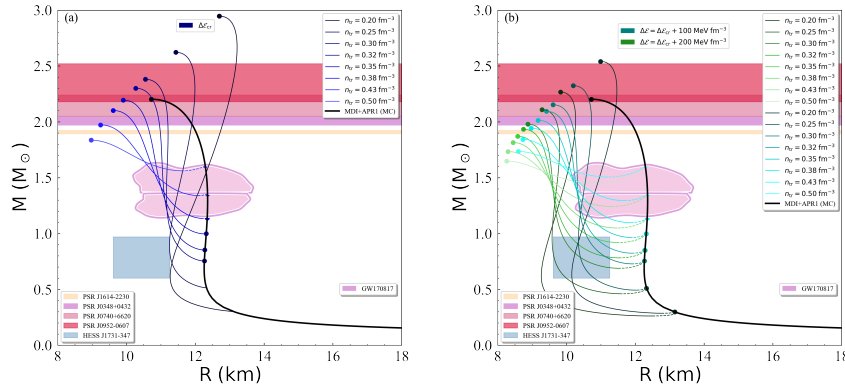
Figure 1. Mass vs Radius diagram for the MDI+APR1 EoS under MC and for a) $\Delta\mathcal{E}_{cr}$, and b) $\Delta\mathcal{E} = \Delta\mathcal{E}_{cr} + 100$ MeV fm^{-3} (blue curves) and $\Delta\mathcal{E} = \Delta\mathcal{E}_{cr} + 200$ MeV fm^{-3} (green curves). The black curve indicates the original EoS. The shaded regions from bottom to top represent the HESS J1731-347 remnant [21], GW170817 event [7], PSR J16142230 [29], PSR J0348+0432 [30], PSR J0740+6620 [31], and PSR J0952-0607 [32] pulsar observations for possible maximum mass.
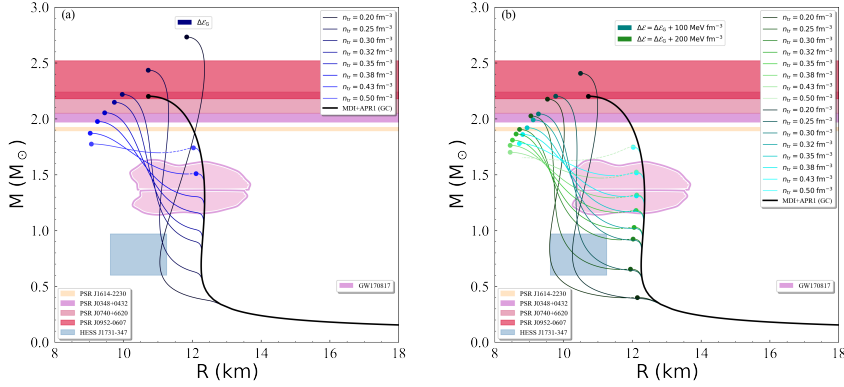
Figure 2. Mass vs Radius diagram for the MDI+APR1 EoS under GC and for a) $\Delta\mathcal{E}_{\mathrm{G}}$, and b) $\Delta\mathcal{E} = \Delta\mathcal{E}_{\mathrm{G}} + 100$ MeV fm^{-3} (blue curves) and $\Delta\mathcal{E} = \Delta\mathcal{E}_{\mathrm{G}} + 200$ MeV fm^{-3} (green curves). The black curve indicates the original EoS. The constraints are the same as in Figure 1.

respectively. Moreover, the constraints on mass and radius of the recently observed remnant HESS J1731-347 have also been included [21].

Figure 3 presents the tidal parameters k_2 and λ of a single neutron star as a function of its mass, for the MDI+APR1 EoS (MC) and for the cases with $\Delta\mathcal{E} = \Delta\mathcal{E}_{\mathrm{cr}} + [100, 200]$ MeV fm^{-3}. The effect of the different $\Delta\mathcal{E}$ and n_{tr} can be observed, as they lead to distinct subbranches.

In Figures 4-5 we present the $\Lambda_1 - \Lambda_2$ space for each EoS and configuration using the observational data of the GW170817 event (orange shaded
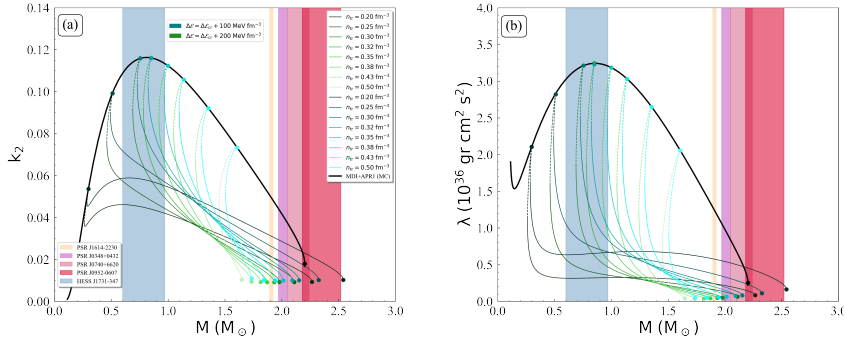
Figure 3. Tidal parameters a) k_2, and b) λ as a relation of the neutron star mass for the MDI+APR1 EoS under MC and for $\Delta\mathcal{E} = \Delta\mathcal{E}_{\mathrm{cr}} + 100$ MeV fm^{-3} (blue curves), and $\Delta\mathcal{E} = \Delta\mathcal{E}_{\mathrm{cr}} + 200$ MeV fm^{-3} (green curves). The black curve indicates the original EoS. The dashed part of curves indicates their unstable region. The constraints are the same as in Figure 1.
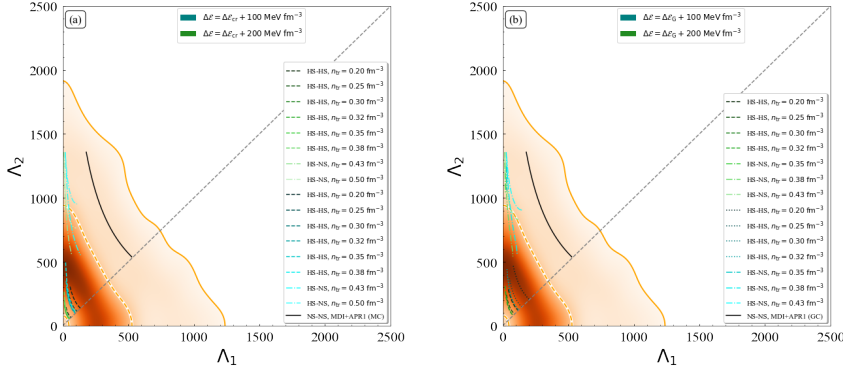
Figure 4. $\Lambda_1 - \Lambda_2$ relation for the MDI+APR1 EoS and a) MC, and b) GC. The black curve indicates the original EoS. For more details see the text.

region) [7]. To be more specific, we considered the three following combinations: Hybrid-Hybrid binary star system (HS-HS), Hybrid-Neutron star system (HS-NS), and finally a Neutron-Neutron one (NS-NS). We notice that we concentrated only in the cases with $\Delta\mathcal{E} = \Delta\mathcal{E}_{\mathrm{cr}} + [100, 200]$ MeV fm^{-3} for MC and $\Delta\mathcal{E} = \Delta\mathcal{E}_{\mathrm{G}} + [100, 200]$ MeV fm^{-3} for GC, because these cases provide more easily a twin star branch on the EoS. The blue curves correspond to $\Delta\mathcal{E} = \Delta\mathcal{E}_{\mathrm{cr}} + 100$ MeV fm^{-3} for MC (GC; $\Delta\mathcal{E} = \Delta\mathcal{E}_{\mathrm{G}} + 100$ MeV fm^{-3}) where the green ones, indicate the $\Delta\mathcal{E} = \Delta\mathcal{E}_{\mathrm{cr}} + 200$ MeV fm^{-3} for MC (GC; $\Delta\mathcal{E} = \Delta\mathcal{E}_{\mathrm{G}} + 200$ MeV fm^{-3}). In all diagrams, the dashed curves correspond to the HS-HS case, the dash-dotted curves to the HS-NS case, and the solid curves to the NS-NS case.
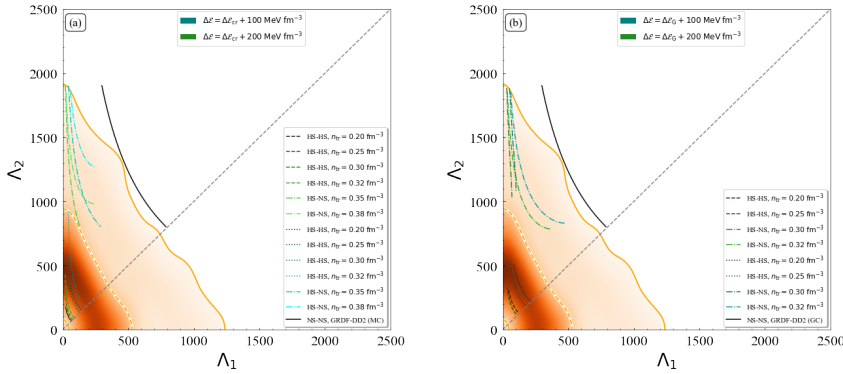
Figure 5. $\Lambda_1 - \Lambda_2$ relation for the GRDF-DD2 EoS and a) MC, and b) GC. The black curve indicates the original EoS. For more details see the text.
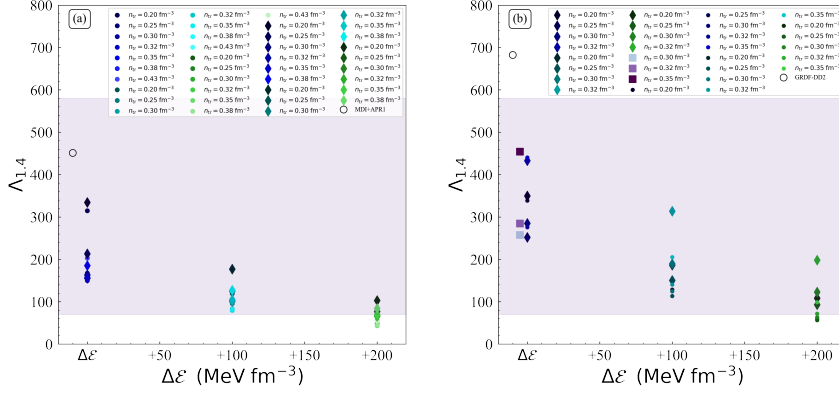
Figure 6. $\Lambda_{1.4} - \Delta\mathcal{E}$ diagram for a single $1.4 M_\odot$ neutron star for a) the MDI+APR1 (left panel), and b) GRDF-DD2 (right panel) EoS for both MC (circles) and GC (diamonds). For more details see the text.

The need for a lower limit on $\tilde{\Lambda}$ that we described before, led us to the exploit of the constrained value of the dimensionless tidal deformability for a single $1.4 M_\odot$ neutron star, derived by the study of the GW170817 event. In Figure 6 we show the relation between $\Lambda_{1.4}$ and $\Delta\mathcal{E}$. We notice that we used only those values of n_{tr} that provide a separate branch from the original EoS. As one can observe, as we move from the $\Delta\mathcal{E}_{cr}$ (and $\Delta\mathcal{E}_G$ for the GC) to higher values of $\Delta\mathcal{E}$ the variation between the marks decreases. In addition, all the marks that correspond to the GC (diamonds) predict higher values of $\Lambda_{1.4}$ compared to the MC, for both EoSs. We notice also that only for the $\Delta\mathcal{E} = \Delta\mathcal{E}_{cr} + 200$ MeV fm^{-3} and $\Delta\mathcal{E} = \Delta\mathcal{E}_G + 200$ MeV fm^{-3} there is a violation of the accepted region. Moreover, in Figure 6(b), the square points indicate the $\Delta\mathcal{E} = \Delta\mathcal{E}_{cr} - 5$ MeV fm^{-3} case under MC and for the GRDF-DD2 EoS. As one can observe, as we move to lower values compared to $\Delta\mathcal{E}_{cr}$, the variation increases, which is in accordance with the behavior that we described before. Furthermore, in order to shed more light on which specific cases should be excluded, we studied the relation between $\Lambda_{1.4}$ and n_{tr}. In Figure 7 we present the aforementioned relation. As a first remark, the MC provides in all cases one more value of n_{tr} compared to the GC. The GC shifts the curves (dashed) to higher values compared to the relevant curves of MC (solid). In addition, as we move to higher values of $\Delta\mathcal{E}$ the curves are shifted to lower values of $\Lambda_{1.4}$.

The left panel of the Figure 7 corresponds to the MDI+APR1 EoS. The curves that correspond to the $\Delta\mathcal{E}_{cr}$ and $\Delta\mathcal{E} = \Delta\mathcal{E}_{cr} + 100$ MeV fm^{-3} lie inside the estimated region. The same holds for $\Delta\mathcal{E}_G$, and $\Delta\mathcal{E} = \Delta\mathcal{E}_G + 100$ MeV fm^{-3}. On the other hand, the solid green curve, which corresponds to the MC with $\Delta\mathcal{E} = \Delta\mathcal{E}_{cr} + 200$ MeV fm^{-3} is excluded. But if we apply the GC, the curve

53
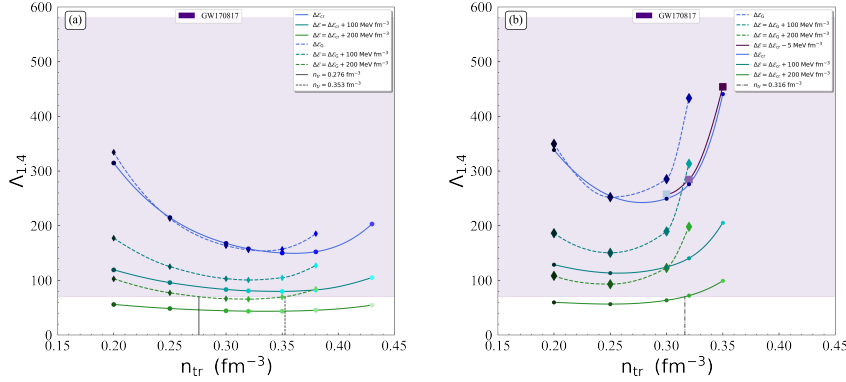
Figure 7. $\Lambda_{1.4} - n_{tr}$ diagram for a single $1.4M_\odot$ neutron star for a) the MDI+APR1 (left panel), and b) GRDF-DD2 (right panel) EoS for both MC (solid lines) and GC (dashed lines). For more details see the text.

is shifted upwards (dashed green curve), with only a part being outside of the estimated region. Hence, not only the kind of construction we choose has a significant role, but the exact value of the transition density affects the final output. Therefore, a further understanding and possible constraints on the transition density n_{tr} are necessary to shed more light on the twin star hypothesis.

The right panel of the Figure 7 corresponds to the GRDF-DD2 EoS. The curves that correspond to the $\Delta\mathcal{E}_{cr}$ and $\Delta\mathcal{E} = \Delta\mathcal{E}_{cr} + 100$ MeV fm^{-3} lie inside the estimated region. Only the green solid curve which corresponds to the MC with $\Delta\mathcal{E} = \Delta\mathcal{E}_{cr} + 200$ MeV fm^{-3} lies outside up to $n_{tr} = 0.316$ fm^{-3}, meaning that above this value even this EoS could be acceptable. All the curves that correspond to the GC lie inside the estimated region. As we mentioned above, the construction and the transition density affect importantly the behavior of the curves. We notice that the purple line indicates the $\Delta\mathcal{E} = \Delta\mathcal{E}_{cr} - 5$ MeV fm^{-3} case under MC. As we have already noticed, as we move to lower values of $\Delta\mathcal{E}$ compared to $\Delta\mathcal{E}_{cr}$, the EoS becomes stiffer, therefore in this diagram the curve is shifted sligtly to higher values of $\Lambda_{1.4}$.

The above results can be summarized as follows: Further systematic theoretical research is required to clarify the role of the method that describes the phase transition in dense nuclear matter, as well as its particular characteristics (density transition, energy, etc.). In addition, more relevant observations from binary neutron star merger (and not only) are necessary to be able to check the plausibility of the theoretical predictions. Possibly, in this case we will be able to confirm, with enough confidence, the existence of twin stars but even more importantly, to confirm, not only qualitatively but also quantitatively, the phenomenon of phase transition in dense nuclear matter.

Acknowledgements

References

[1] N.K. Glendenning, *"Compact stars - Nuclear physics, Particle physics and General Relativity"* (Springer, 1997).

[2] P. Haensel, A.Y. Potekhin, and D.G. Yakovlev, *"Neutron Stars 1: Equation of State and Structure"* (Springer-Verlag, New York, 2007).

[3] J. Schaffner-Bielich, *"Compact Star Physics"* (Cambridge University Press, Cambridge, England, 2020).

[4] F. Weber, *"Pulsars as Astrophysical Laboratories for Nuclear and Particle Physics"* (U.K.: Institute of Physics, Bristol, 1999).

[5] B.P. Abbott *et al.*, *Phys. Rev. Lett.* **119** (2017) 161101.

[6] B.P. Abbott *et al.*, *Phys. Rev. Lett.* **121** (2018) 161101.

[7] B.P. Abbott *et al.*, *Phys. Rev. X* **9** (2019) 011001.

[8] M.G. Alford, S. Han, and M. Prakash, *Phys. Rev. D* **88** (2013) 083013.

[9] J.E. Christian, A. Zacchi, and J. Schaffner-Bielich, *Eur. Phys. J. A* **54** (2018) 28.

[10] G. Montana, L. Tolos, M. Hanauske, L. Rezzolla, *Phys. Rev. D* **99** (2019) 103009.

[11] U.H. Gerlach, *Phys. Rev.* **172** (1968) 1325.

[12] Kämpfer, *J. Phys. A: Math. Gen.* **14** (1981) L471.

[13] Kämpfer, *Phys. Lett. B* **101** (1981) 366.

[14] N.K. Glendenning, C. Kettner, *Astron. Astrophys.* **353** (2000) L9L12.

[15] K. Schertler, C. Greiner, J. Schaffner-Bielich, and M.H. Thoma, *Nucl. Phys. A* **677** (2000) 463.

[16] D. Blaschke, D.E. Alvarez-Castillo, and S. Benic, [arXiv:1310.3803].

[17] D.E. Alvarez-Castillo and D. Blaschke (2013), arXiv:1304.7758.

[18] S. Benic, D. Blaschke, D.E. Alvarez-Castillo, T. Fischer, and S. Typel, *Astron. Astrophys.* **577** (2015) A40.

[19] D.E. Alvarez-Castillo and D. Blaschke, *Phys. Part. Nucl.* **46** (2015) 846.

[20] D.E. Alvarez-Castillo, A. Ayriyan, S. Benic, D. Blaschke. H. Grigorian, and S. Typel, *Eur. Phys. J. A* **52** (2016) 69.

[21] V. Doroshenko, V. Suleimanov, G. Phlhofer, and Andrea Santangelo, *Nat. Astron.* (2022).

[22] Z.F. Seidov, *Soviet Astronomy* **15** (1971) 347.

[23] S. Postnikov, M. Prakash, J.M. Lattimer, *Phys. Rev. D* **82** (2010) 024016.

[24] E.E. Flanagan, T. Hinderer, *Phys. Rev. D* **77** (2008) 021502(R).

[25] T. Hinderer, *Astrophys. J.* **677** (2008) 1216.

[26] T. Hinderer, B.D. Lackey, R.N. Lang, J.S. Read, *Phys.Rev. D* **81** (2010) 123016.

[27] P.S. Koliogiannis and Ch.C. Moustakidis, *Astrophys. J.* **912** (2021) 69.

[28] S. Typel, *J. Phys. G: Nucl. Part. Phys.* **45** (2018) 114001 (17pp).

[29] Z. Arzoumanian, A. Brazier, S. Burke-Spolaor, *et al.*, *Astrophys. J. Suppl. S.* **235** (2018) 37.

[30] J. Antoniadis, P. Freire, N. Wex, *et al.*, *Sci.* **340** (2013) 448.

[31] H. Cromartie, E. Fonseca, S. Ransom, *et al.*, *Nat. Astron.* **4** (2020) 72.

[32] R.W. Romani, D. Kandel, A.V. Filippenko, T.G. Brink, and W. Zheng, *Astrophys. J. Lett.* **934** (2022) L17.